Influence of Anthropometric Variation of the Lower Extremities on Injury Severity in a Real-world Far-side Crash: A Sensitivity Study

Sonja Fitterer, Desiree Kofler, Felix Ressi, Hermann Steffan, Corina Klug

Abstract This study examines the influence of anthropometric variability on lower extremity injury mechanisms in far-side crashes using Human Body Model (HBM) simulations. A real-world far-side crash was reconstructed, including full-scale crash tests to derive a realistic crash pulse. In the real-world crash, the female driver sustained a fracture of the proximal tibia, which is why the interaction of the legs with the instrument panel was in focus for the HBM simulations.

To validate the material properties of the instrument panel, pendulum impact tests were conducted on the physical car model. The car seat was 3D scanned and incorporated into the simulations. Based on a Bayesian linear regression model with target values from an anthropometric database, the VIVA+ 50F was morphed to different lower extremity bone lengths within the 50th percentile female. These morphed HBMs were used for simulations of the far-side crash scenario. The simulations showed a clear relationship between tibial length and cortical strain values, providing a reference for tibial injury risk. A direct, statistically significant relationship between the variation in lower extremity bone length and principal strains in both the tibia and femur was observed. These results emphasise the importance of considering anthropometric differences for occupant safety.

Keywords Accident reconstruction, anthropometry, human body models, lower extremity injury, occupant safety.

I. INTRODUCTION

According to the European New Car Assessment Programme (Euro NCAP) 2030 Vision [1], lateral collisions account for roughly 25% of all road crashes, underscoring their continued relevance in occupant safety assessments. Lower extremity injuries, particularly those affecting the femur, knee, tibia, and foot, are frequently observed in side collisions and may result in long-term functional limitations, even when classified as moderate in severity (Abbreviated Injury Scale (AIS) 1–3) [2-4]. While past research has focused primarily on near-side collisions, far-side impacts, where the occupant is seated opposite the side of impact, have gained increased attention. Several studies have demonstrated that current anthropomorphic test devices (ATDs), such as the Worldwide Harmonized Side Impact Dummy (WorldSID), exhibit limitations in replicating human kinematics and injury responses in far-side crashes [5-9]. According to Euro NCAP, nearly half of all injured occupants in side collisions are located on the far-side [10]. As previous studies have demonstrated the relevance of far-side crashes for occupant injury mechanisms [11], Euro NCAP introduced far-side protection as part of its rating system in 2020 and subsequently selected this load case as the first pilot scenario for virtual testing of occupant safety [5][10][12]. Reference [13] further showed that serious injuries still occur in real-world side impacts, even in vehicles with high side-impact protection ratings, underscoring the need for improved assessment tools.

Human Body Models (HBMs), in contrast, have shown higher biofidelity and the ability to capture internal load distributions, offering advantages in the analysis of diverse anthropometries [14-15]. HBMs allow detailed investigations of regional injury types and enable analysis across sex- and anthropometry-specific variations not represented by current ATDs [16]. However, harmonised and reliable assessment procedures for HBMs in far-side impacts are still under development [5]. One key challenge lies in capturing the real-world variability in human morphology and seating position. Studies using the ANSUR-II database and Bayesian modelling approaches have demonstrated that body height, limb length, and Body Mass Index (BMI) have a direct influence on impact

Sonja Fitterer is a PhD student in Biomechanics (+43 316 87330367, s.fitterer@student.tugraz.at), D. Kofler is a Project Assistant, F. Ressi is a Senior Scientist, H. Steffan is Professor and C. Klug is Associate Professor at the Vehicle Safety Institute of Graz University of Technology, Austria

kinematics and local loading [17]. Reference [18] already emphasised the need for a systematic re-evaluation of side impact protection concepts, underlining limitations of traditional testing setups in capturing emerging injury mechanisms.

The methodological integration of real-world crash data with HBMs increasingly enables realistic predictions of occupant injuries. Reference [19] recently demonstrated the efficiency of a systematic methodology comprising crash reconstruction via finite element models, estimation of occupant loading, simulation of occupant kinematics with HBMs, and subsequent injury analysis. This approach reliably reproduced real-world injury patterns. The researchers' conclusions emphasise that detailed reconstruction of individual accident scenarios offers significant insights into specific injury mechanisms, aligning closely with the objectives of the present study.

The aim of this study is to systematically assess how variations in tibial and femoral lengths among 50th percentile female occupants influence injury severity in far-side crash scenarios. Specifically, the study seeks to quantify the relationship between length variability of the lower extremities and tibial strain values, thereby improving understanding of anthropometry-related injury mechanisms and supporting the development of more inclusive occupant safety assessment protocols for one real-world far side crash reconstructed in detail.

II. METHODS

This study combined accident reconstruction, experimental testing and numerical simulation. The aim was to systematically investigate the influence of anthropometric characteristics of the lower extremity bone lengths on injury mechanisms in far-side impacts.

Baseline was the reconstruction of a real-world far-side crash between a Volkswagen Polo V (2013) and a Peugeot 307 SW (2005), with the VW Polo being the far-side vehicle. The collision was reconstructed using PC-Crash [20], to determine crucial crash parameters. The reconstruction results formed the basis to reproduce the far-side crash using identical vehicles under controlled real-world conditions. To ensure a realistic representation of the vehicle interior in the Finite Element (FE) simulations, material properties of the instrument panel (IP) were validated through experimental testing and geometries adjusted. Since the far-side occupant was a 58-year-old female who sustained a lateral condylar fracture of the right tibia in the crash, the HBM, VIVA+ 50F-seated, was selected as the base HBM for the simulation study due to the known sex [15]. While no further anthropometric data were available beyond age and sex, the 50th percentile female representation was adopted as a reasonable approximation. To investigate the sensitivity of tibial injury risk to interpercentile lower extremity length proportions, the total leg length was fixed. This approach enabled a focused analysis on how variations in tibia-to-femur bone length proportions influence the tibial injury risk, independent of overall leg length.

A Bayesian linear regression model was developed [21] to derive variations in leg length, within the range of a 50th percentile female, based on anthropometric data [17]. On this basis, a total of eight leg configurations of the VIVA+ 50F model were generated to analyse the influence of differences in tibia and femur lengths on the biomechanical load on lower extremities. The prepared HBMs, together with the new seat model and validated IP, were integrated into a generic vehicle interior (GVI) model [22] and subjected to the identical real-world far-side impact scenario.

Experimental Testing and Characterisation

After the accident reconstruction with PC-Crash delivered crash parameters such as principal direction of force (PDOF) and impact velocities, the concerned far-side crash was replicated in a crash test with identical vehicles based on the reconstruction results. In accordance with the Euro NCAP protocol [23], triaxial acceleration and angular rate sensors were used and positioned in the vehicles. Several high-speed cameras were positioned in different external perspectives to document the relative motion behaviour of both vehicles. In addition, cameras in the vehicle interior recorded kinematics and any deformations of the occupant compartment. The combination of interior and exterior perspectives allowed a comprehensive kinematics and load analysis. The data obtained made it possible to derive a realistic crash pulse and the change in velocity (ΔV) of the far-side vehicle. Figure 1 provides an overview of the physical crash from a top perspective. Figure 2 shows the maximum intrusion of the Peugeot into the side of the Polo from a frontal view, a key moment for the subsequent analysis of the load situation on the lower extremities. The results of the crash test provided the necessary crash parameters and other boundary conditions for a realistic simulation setup.

Fig. 1. Physical crash test – top view.

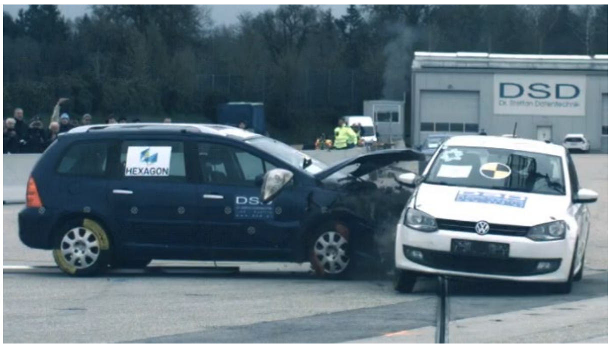

Fig. 2. Physical crash test – frontal view.

To be able to assess the injury kinematics of the proximal tibia, the contact forces of the tibia with the instrument panel had to correspond to the real-world crash. Therefore, pendulum impact tests were carried out to validate the material of the instrument panel. The aim was to analyse the material behaviour of relevant contact areas between the proximal tibia and the instrument panel of the VW Polo under controlled conditions. The test setup is shown in Figure 3. An identical vehicle was used for the test. To carry out the pendulum tests, the left side structure of the vehicle was removed. A steel impactor with a hemispherical front surface was used, which was geometrically adapted to the lateral proximal tibia of the VIVA+ 50F seated HBM. The impactor was equipped with a trigger for exact data measurement at the front and attached to a steel tube. A load cell integrated between the tube and the impactor head recorded impact forces precisely and synchronised with time (Fig. 4).

Fig. 3. Experimental setup pendulum tests.

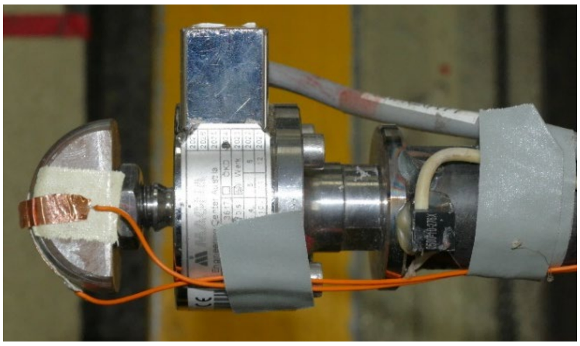

Fig. 4. Pendulum assembly.

To ensure precise material validation, an impact matrix with a total of nine measuring points was defined to cover all possible contact surfaces of the lower extremity with the instrument panel. During the test, the pendulum was guided against the instrument panel from the driver's side in accordance with the impact matrix (Fig. 5).

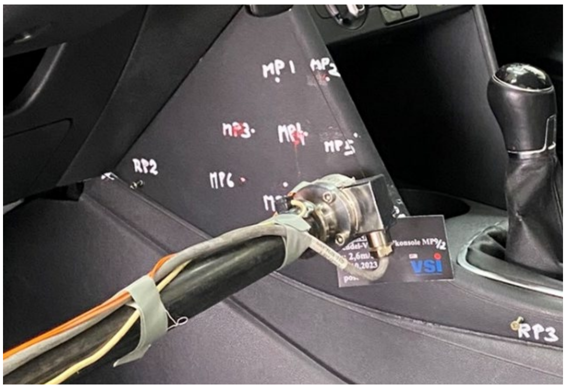

Fig. 5. Impactor and impact matrix on instrument panel.

The impact velocity of the impactor was 2.6 m/s and was determined on the basis of a previous simulation study of the real-world crash [24]. High-speed cameras recorded the test runs. The force-time curves and maximum intrusions recorded during the pendulum tests were used to characterise the material of the instrument panel in the generic vehicle model. Differences in local stiffness were taken into account in the material definition depending on the location in order to simulate the non-linear structural behaviour as realistically as possible. The curves from the test and from the simulations were validated in accordance with ISO/TS 18571:2024 [25]. All validation curves with ISO scores can be found in Appendix A.

In addition, to retrieve the precise geometry of the original VW Polo seat, a 3D scan was conducted using a Creaform MetraScan (Germany) device. The 3D scan enabled the exact geometry of the real seat to be digitised in high resolution. The captured surface data was transferred into a fine-mesh surface model. With the ANSA hexa block method, the mesh surface model was converted to small cuboids for generating the FE mesh. The FE model of the Polo seat was then integrated into the generic vehicle interior model. The material properties of the seat from the original GVI model were retained (Fig. 6).

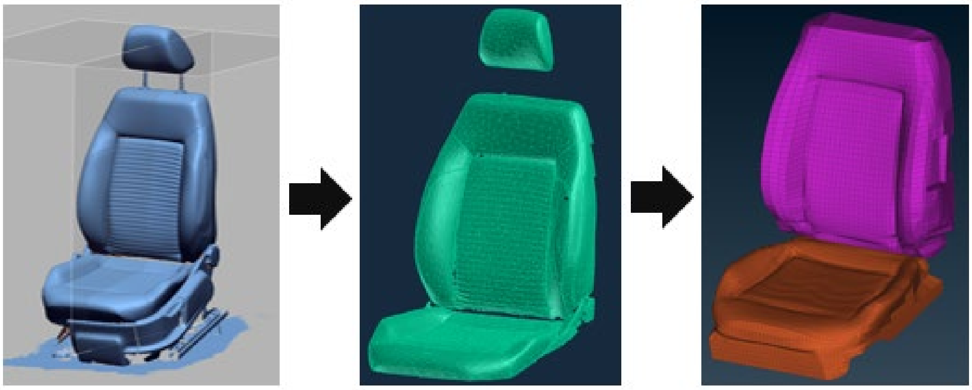

Fig. 6. Development of FE seat model.

Anthropometric Analysis

To quantitatively evaluate the influence of length variability in lower extremities, a Bayesian linear regression model was developed [21]. While Bayesian models offer versatility, their primary advantage is their ability to produce posterior predictive draws. These draws effectively simulate a large population sample, capturing both individual anthropometric variability and model uncertainty. The objective was to predict realistic tibial and femoral lengths for females at the 50th percentile using data from the Anthropometric Survey of U.S. Army Personnel II (ANSUR II) Female dataset [17]. Since the ANSUR II Female dataset did not provide a direct measurement of the tibial length, this variable was derived by subtracting the *Lateral Malleolus Height* from the *Tibial Height* for each subject (Fig. 7). The *Lateral Malleolus Height* is defined as the vertical distance between a standing surface and the lateral malleolus. *Tibial Height* refers to the distance from the standing surface to the superior most prominent point on the medial condyle of the right tibia (tibiale landmark) [26]. Both measurements are included in the ANSUR II Female dataset [27].

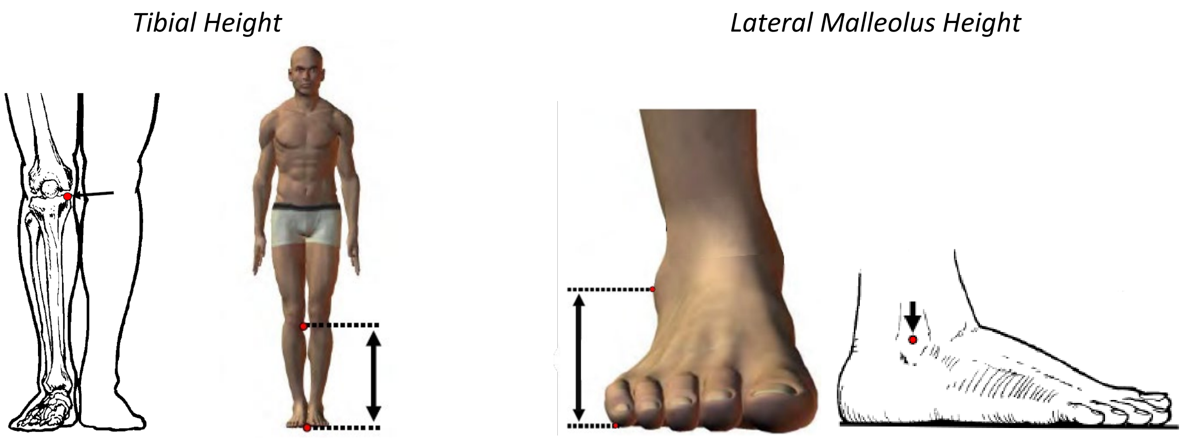

Fig. 7. Measurement landmarks used to calculate the tibial length.

The Bayesian linear regression model was given as:

$$L_T = \alpha + \beta \cdot (H - H_{mean}) + \gamma \cdot (BMI - BMI_{mean}) + \varepsilon, \quad (1)$$
$$\alpha \sim Normal\,(mean, 10), \beta \sim Normal\,(0,1), \gamma \sim Normal\,(0,1), \sigma \sim Uniform\,(0,10),$$

where L_T was the predicted tibial length (mm), H was body height (mm), BMI was Body Mass Index (kg/m²), α, β, γ were regression coefficients (-) and $\varepsilon \sim \mathcal{N}(0, \sigma)$ was the normally distributed error term (-).

This modelling approach utilised tibial length (LT), measured in millimetres, as the dependent variable, incorporating height (H) and body mass index (BMI) as continuous predictor variables. The priors for α, β, and γ were normally distributed, with α centred around the mean anthropometric measure of the dataset. The analysis was limited to 1,986 female participants from the ANSUR II dataset.

Human Body Model Simulations

As stated above, seven statistically representative tibial lengths and resulting femur lengths within the female 50th percentile population were determined from the estimates of the Bayesian linear regression model. These values were applied to morph the lower extremities of the VIVA+ 50F seated HBM to produce unique model configurations. The mesh morphing process was performed using a customised python-based morphing tool developed at TU Graz based on the Python Geometrical Morphing – PyGeM library [28] using radial basis functions. This tool modifies the nodal coordinates of the finite element mesh along the longitudinal axis of the bones, achieving the desired lengths of the femoral and tibial segments while maintaining mesh continuity and topology. In total, the original VIVA+ 50F seated HBM model and the seven morphed HBMs resulted in eight HBM configurations, which were used for the simulation study (Fig. 8). Tibial length increases from Model 1 to Model 8, while femoral length decreases, representing a realistic anthropometric range with the 50th percentile female population.

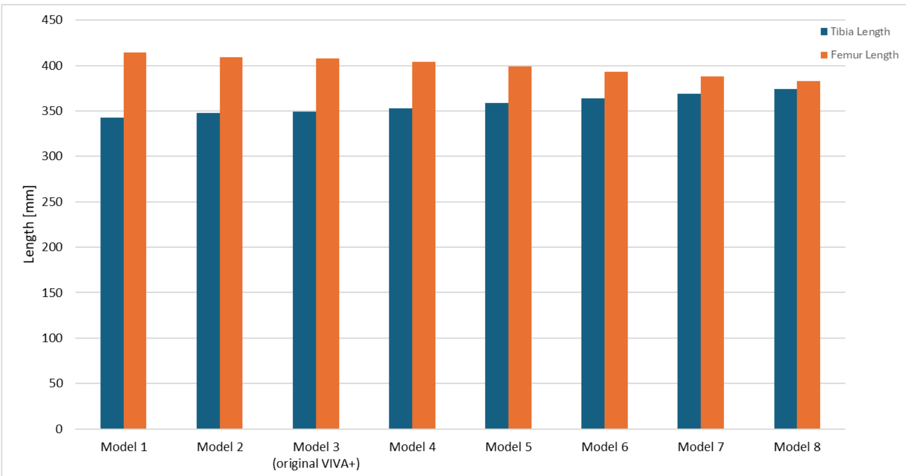

Fig. 8. Variation in femoral and tibial lengths across eight VIVA+ 50F seated variants.

The material properties of the VIVA+ tibia remained unchanged. The cortical bone is modelled with MAT_PLASTICITY_COMPRESSION_TENSION with properties based on [29]. The trabecular bone is also modelled with MAT_PLASTICITY_COMPRESSION_TENSION based on [30] All material properties are openly accessible in the VIVA+ models and related publications [15].

Finally, the simulation study was subsequently performed using three fundamental components: the real-world far-side crash parameters (PDOF, ΔV, crash pulse), validated IP material properties and the original seat geometry. Eight VIVA+ 50F seated HBMs with different femoral and tibial length configurations, while maintaining a constant overall leg length, were created and used for the simulations. This setup enabled a controlled sensitivity analysis on how lower extremity length variations affect regional strain distributions and injury risk. The simulations were carried out with LS-Dyna R12.2 (single precision, MPP build). The simulation results were analysed with the python library Dynasaur [31].

The overall rib fracture risk was evaluated using the strain-based rib fracture risk function according to [32] for the age of 50 years.

III. RESULTS

Anthropometric Analysis

Based on the 95% density interval (HDI) for tibial length derived from the Bayesian linear regression model (342.66–395.18 mm), a sequence of tibial lengths was determined. This was accomplished by dividing the range (maximum - minimum tibial length) by 10, resulting in increments of 5.25 mm. Consequently, 10 incremental tibial lengths were generated. However, one length was substituted with the original VIVA+ 50F tibial length values, and two lengths were excluded as they exceeded the anthropometric constraints associated with the femoral dimensions of the 50th percentile female. In order to maintain a constant total leg length that conforms to the anthropometric standards within the 50th percentile female population, across all HBM configurations, the combined length of the femur and tibia was fixed at 757.03 mm, which is the original length value from the VIVA+ 50F seated model. For each tibial length selected from the Bayesian linear regression range, the corresponding femoral length was calculated by subtracting the tibial length from the fixed total. This approach created a controlled variation in tibia-to-femur proportion while ensuring that the overall leg length remained representative of a 50th percentile female. By varying only the internal segment proportions, the influence of tibia/femur length ratio on injury response could be isolated without confounding effects from changes in total leg length. This procedure ensured that all resultant leg lengths conformed to anthropometric standards within the 50th percentile female population.

Detailed results and supporting graphs for the Bayesian approach are provided in Appendix B.

Human Body Model Simulations

In the far-side crash simulations, tibial loading and strain distribution varied noticeably with varying lengths of tibia and femur (Table I). All models exhibited principal strains in the cortical bone of the right tibia that were within or close to the range of experimentally derived fracture thresholds reported by [29] for individuals aged 40–89 years (0.0227-0.0305). The maximum 99th percentile strain observed was 0.0338 for the morphed HBM with the longest tibia (374.16 mm), while the minimum was 0.0217 for the morphed HBM with the shortest tibia (342.66 mm). All maximum principal strains can be found in Appendix C.

TABLE I
MEASURED TIBIAL CORTICAL STRAINS (99TH PS)

Tibial Length [mm]	Resulting Femoral Length [mm]	Measured Strain Value [-]
342.66	414.37	0.021732282
347.91	409.12	0.022724119
349.16	407.87	0.023916147
353.16	403.87	0.025227242
358.41	398.62	0.028485817
363.66	393.37	0.030734349
368.91	388.12	0.031832392
374.16	382.87	0.033837854

The highest strains were detected shortly after initial contact with the instrument panel. Appendix D summarises the contact kinematics of the right tibia with the instrument panel. Differences in the point of impact and contact trajectory on the instrument panel resulted in changes in the kinematics and y-force on the lateral condyle of the right tibia, depending on the tibial length. The trend towards lower loads on the tibia with shorter tibial lengths can also be observed here.

Figure 9 shows that the highest strains are found on the lateral condyle of the proximal tibia, which is congruent with the reported condyle fracture in the real-world crash. Furthermore, the strains decrease as the tibia length decreases.

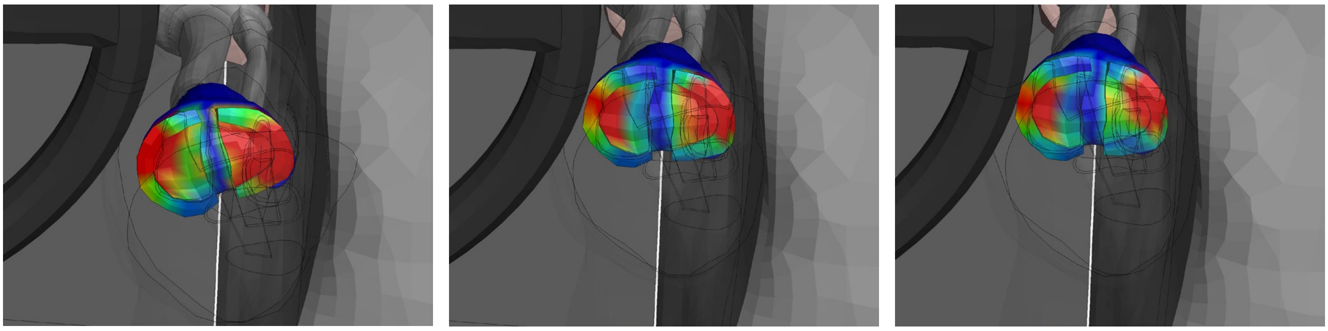

Fig. 9. Fringe plots of the right proximal tibiae (long, original, short) upon contact with the instrument panel.

All eight simulation setups showed a confirmed fracture risk with the tibia shaft fracture risk curve (Appendix C).

A linear regression analysis was performed to examine the relationship between tibial length and the 99th percentile principal strain in the cortical region of the right tibia. Additionally, a series of linear regression analyses were conducted to evaluate the influence of tibial length on 99th percentile principal strain values in three cortical regions (proximal, middle, and distal) of the right femur shaft. For the strains in the cortical bone of the tibia, the analysis yielded a regression equation with a slope of 0.0004094 and an intercept of –0.011895, indicating a strong positive association: as tibial length increases, strain values in the cortical bone rise accordingly (Fig. 10).

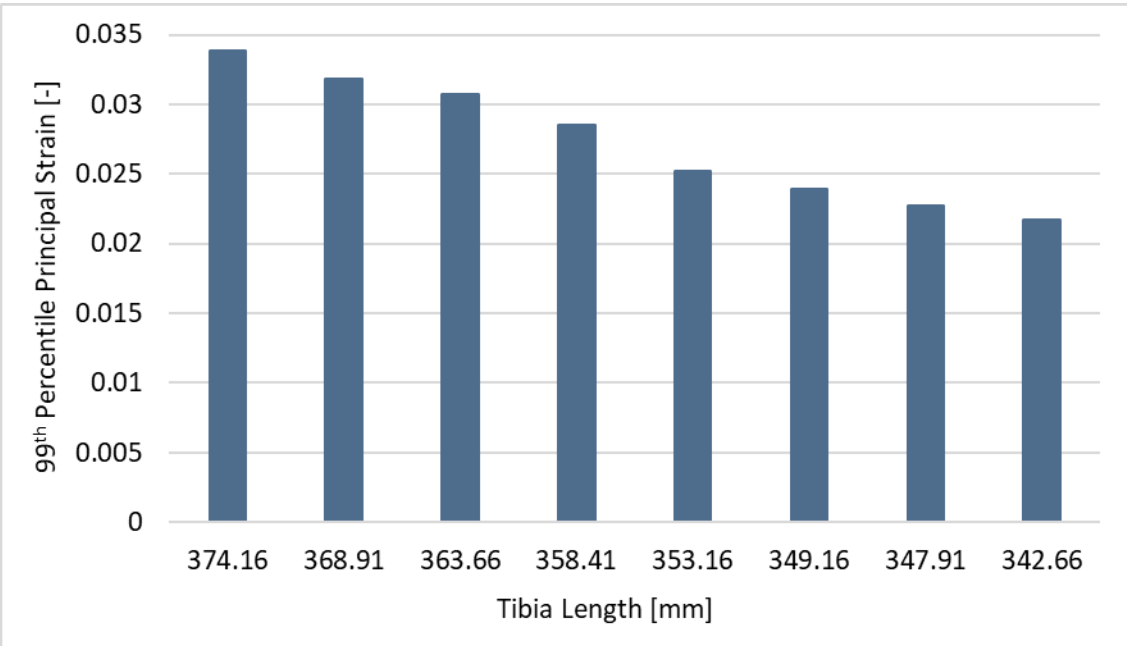

Fig. 10. Principal strains in cortical bone of right tibia over different leg length configurations.

The coefficient of determination (R^2) was 0.984, signifying that 98.4% of the variance in cortical strain can be explained by tibial length. This relationship was found to be statistically significant ($p = 0.00000121$), with a standard error of 2.11×10^{-6}.The fit line, derived from the regression model, represents the best linear approximation of the observed data and provides a predictive model for estimating strain based on tibial dimensions (Fig. 11). The high R^2 value and low p-value together confirm that tibial length exerts a statistically significant influence on cortical strain under the examined loading conditions.

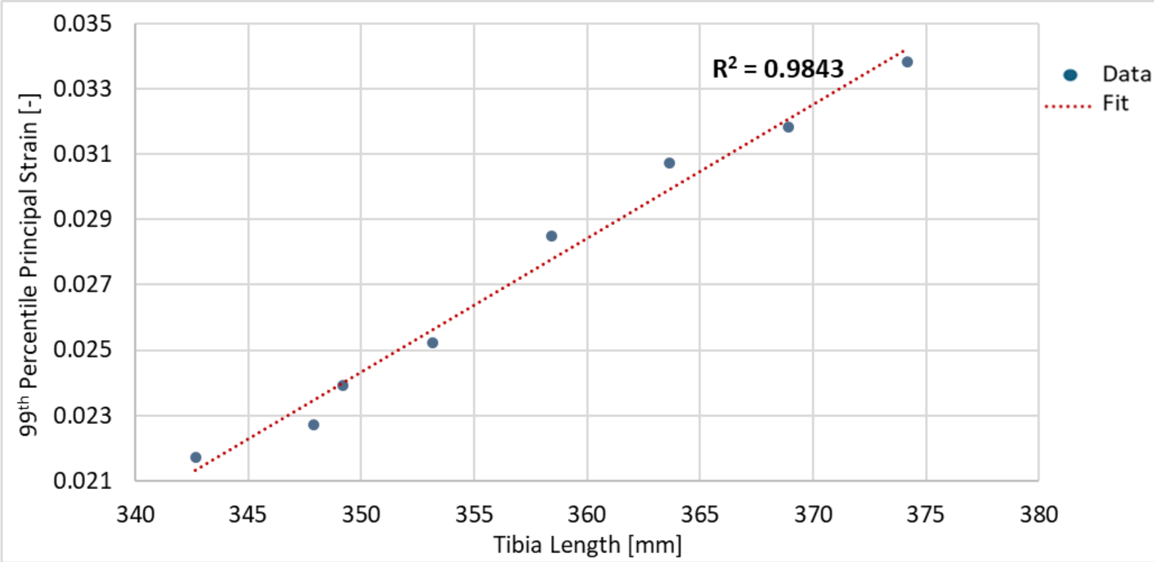

Fig. 11. Tibial length vs. tibial cortical-R 99th percentile principal strain.

For the femora, across all regions, tibial length showed a positive relationship with femoral strain, indicating that longer tibiae, with resulting shorter femora, tend to be associated with higher strain magnitudes under simulated loading conditions. The strongest relationship was observed in the distal shaft region, where tibial length explained 97.1% of the variance in strain (R^2 = 0.971) with a statistically significant effect (p = 0.000051). In contrast, the associations for the proximal (R^2 = 0.658, p = 0.072) and middle (R^2 = 0.519, p = 0.183) regions were weaker and did not reach statistical significance.

All results of the statistical assessment are summarised in Table II.

TABLE II
STATISTICAL ASSESSMENT

	Right Tibial Cortical Strain vs. Tibial Length		
Region	Slope	R^2	p-value
Cortical bone	0.0004094	0.9843	0.00000121
	Right Femoral Cortical Strains vs. Tibial Length		
Region	Slope	R^2	p-value
Proximal	0.0001205	0.658	0.072
Middle	0.0002481	0.519	0.183
Distal	0.0003074	0.971	0.000051

Another interesting observation was that variations in tibia length led to noticeable differences in overall rib fracture risks (Fig. 12). The relationship between tibia length and rib fracture risk was examined across different Number of Fractured Ribs (NFR = 0, 1, 2, and 3+) levels. The results indicated that individuals with shorter tibia lengths tend to have a higher risk of sustaining at least one rib fracture, with the highest risk observed for NFR=1. Specifically, fracture risk of NRF=1 peaked at a tibia length of 347.91mm (62.24%) and decreased with increasing tibia length (36.45% for 374.16 mm tibial length), In contrast, fracture risks for the NFR = 2 and NFR = 3+ were more moderate and showed less consistent trends across tibia lengths. While for NFR=2, the fracture risks were ranging between 25.15% and 42.73%, without a strong directional trend, a slight increase in risk was noted in mid-range tibia lengths (353.16 - 363.66 mm). Overall, the fracture risk for NFR=3+ was lower than for NFR=1 and NFR=2, dropping to <10% for some tibial lengths. But for 353.16mm tibial length, the NFR=3+ fracture risk was higher than the NFR=1 fracture risk.

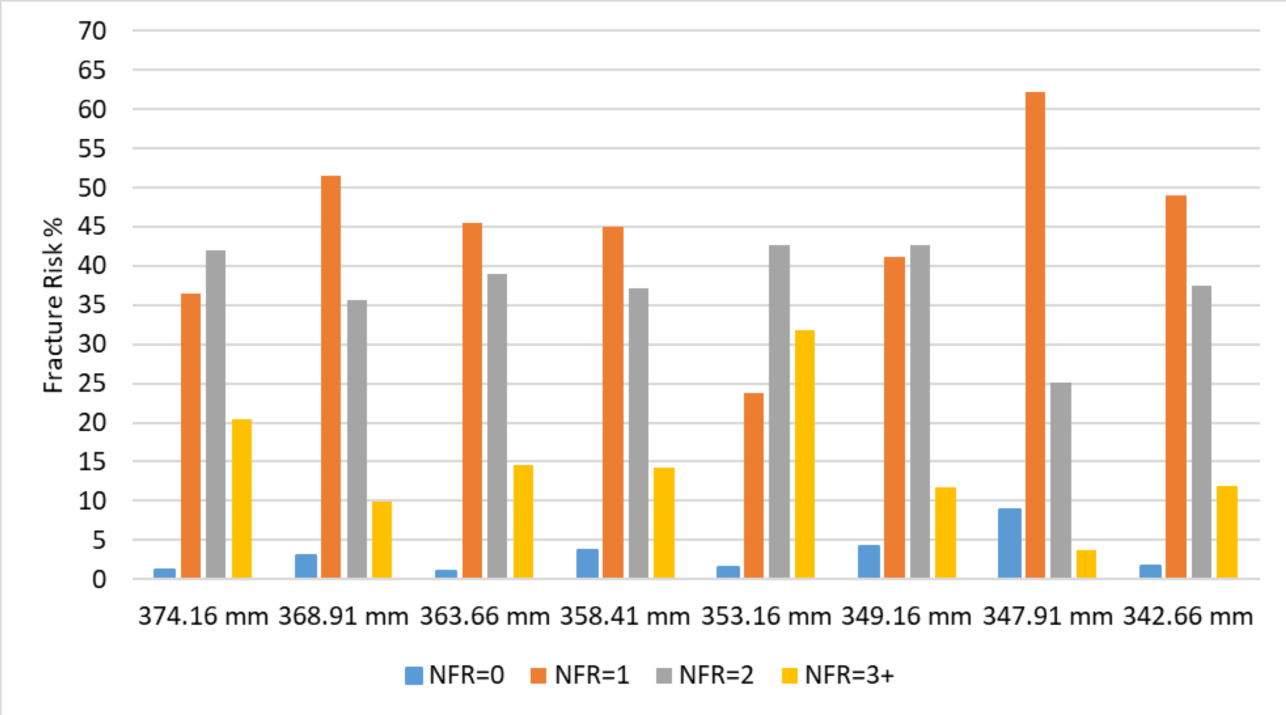

Fig. 12. Overall rib fracture risk across four Number of Fractured Ribs (NFR) levels for different tibial lengths.

IV. DISCUSSION

All morphed VIVA+ 50F HBMs were subjected to the same far-side crash conditions using the validated material parameters and boundary conditions. The parametric length variation of the lower extremities (tibia with resulting femur length) allowed a controlled sensitivity analysis regarding internal force distribution, regional fracture risk, and biomechanical implications of tibial length variability. The results demonstrate that tibial length has a statistically significant influence on cortical strain magnitude of the tibia. Additionally, tibial length exerted a region-specific influence on femoral cortical strain, with the distal femur showing the most pronounced and statistically robust sensitivity.

This suggests that longer tibiae/shorter femora increased right tibial and regional femoral loading due to altered impact force distribution on the instrument panel. Comparison with age-specific fracture thresholds from [29] showed that while the peak simulated strain in the right tibial cortical bone (0.0338) was below the average young adult fracture strain (~0.039), the measured strains exceeded the fracture threshold for individuals aged 60–89 years. Although [29] did not detect statistically significant age-related differences in fracture strain, they did report a general decline in mechanical properties with age. Given that the simulated far-side occupant represented a 58-year-old female, the observed strain values (0.0217-0.0338) in the cortical tibia are relevant and contextually appropriate, as [29] reported true strains at fracture points between 0.0227 and 0.0266 for individuals aged 60–89, and 0.0286 to 0.0305 for individuals aged 40–59. Thus, the simulated strains fall within or near the experimentally observed failure range for older adults.

The highest cortical bone strains in the right tibia were observed shortly after initial contact with the instrument panel, indicating that this moment is critical in the injury mechanism. Appendix D provides a detailed overview of the tibia–instrument panel contact kinematics, revealing that variations in the point of impact and contact trajectory on the panel were influenced by tibial length. Specifically, shorter tibiae tended to experience lower lateral (y-direction) forces on the lateral condyle, consistent with a general trend towards reduced tibial loading in individuals with shorter tibial lengths. Conversely, longer tibiae exhibited increased y-displacement during contact, with a linear relationship observed between tibial length and y-displacement. This may be partly attributed to the greater mass and inertia associated with longer tibiae. Despite this potential confounding factor, the observed kinematic trends are consistent with the overall strain distribution findings. The data suggest that tibial length affects the contact kinematics in a way that alters both the location of impact on the instrument panel and the tibial trajectories. In combination with the geometric features of the instrument panel, these variations contribute to differences in local loading conditions and, consequently, to the cortical bone strain responses.

The observed overall rib fracture risks imply that tibial length was a contributing factor in rib fracture occurrence, especially for a single fractured rib (NFR = 1), where the highest risks were observed for shorter tibial lengths. While the patterns for multiple rib fractures (NFR = 2 and NFR = 3+) were less consistent, a slight increase in risk was noted for some mid-range tibial lengths. One exception was seen at 353.16 mm, where the NFR = 3+ risk exceeded that of NFR = 1. This observation may point to more complex relationships between anthropometric variation and injury outcomes.

Despite the fact that, based on the fracture risk curves, all tibiae suffered a fracture, it should be emphasised that since the tibial length has a significant influence on the strains in the cortical bone, it can be assumed that anthropometries outside the 50th percentile will also be affected by this correlation. Moreover, as all examined leg configurations revealed a definite risk of injury, the HBM's injury prediction appears particularly robust, namely with regard to lower extremity injuries in far-side crash scenarios. In addition, the simulations in the study were analysed with a risk curve for the tibial shaft due to the lack of a risk curve for the proximal tibial region. Test data would be needed in this area to develop a specific risk curve for the proximal tibia.

In a prior pre-study conducted by [24], key parameters influencing injury risks in the same baseline far-side crash scenario were identified, notably changes in impact velocity (ΔV), pulse duration and principal direction of force (PDOF). The results from that study highlighted that even minor variations in crash severity parameters (such as ΔV and pulse duration) influenced the injury risk, particularly in the tibia and head (Head Injury Criterion (HIC) 15). Specifically, tibial injury risk increased when ΔV exceeded certain thresholds, underscoring the critical role of accurately reproducing crash pulse characteristics to predict realistic injury outcomes.

In the current study, building upon these previous insights, the effect of anthropometric variability, particularly tibial and femoral length, was examined in greater depth. Given that the previous findings demonstrated sensitivity to slight changes in boundary conditions, it was crucial to isolate leg length variations while controlling other parameters rigorously. Consequently, the detailed validation of instrument panel material properties and precise reproduction of seat geometry were essential steps taken in the present analysis to minimise uncertainties identified earlier. This methodological refinement enabled a clearer understanding of how interpercentile variability independently influences lower extremity injury risk, enhancing the specificity and robustness of occupant safety assessments. The findings show that specific crash and occupant data, as well as precise seat geometry, significantly influence load in the lower extremities. Similar observations were reported by [19] who demonstrated that minor variations in intrusion, crash pulse, and impact angle could lead to markedly different injury patterns. This underlines the validity of present simulation results with regard to the effects of anthropometric variability. Collectively, these studies highlight the importance of comprehensive accident reconstruction, precise boundary condition replication, and consideration of anthropometric diversity in evaluating occupant injury mechanisms.

The results have implications for understanding the risk of injury associated with anthropometric variation in lower extremities in far-side impacts. A limitation of the study is the lack of material characterisation of the seat. Although geometric adjustment has shown a significant effect, the material properties of the seat should also be recognised as an influencing factor and included in future research. Furthermore, no height or weight data were available for the real-world case beyond age and sex. As such, the 50th percentile female representation was used as a reference configuration. This introduces uncertainty regarding anthropometric accuracy, but ensures demographic plausibility. The posture of the lower extremities was held constant across all morphed HBM configurations. While this approach was necessary to isolate the effects of tibial and femoral segment length variation, it omits potential interactions between posture and injury risk. Previous research has demonstrated that joint angles affect lower limb kinematics and impact loading patterns. As such, posture variation represents an important next step in assessing tibial fracture mechanisms under real-world conditions, particularly given the likely diversity in natural seating configurations among occupants. Future studies should include additional variation effects, such as seat position, and further material validation, such as seat property analysis. Another consideration should be the development of proximal tibia-specific risk curves.

V. CONCLUSION

This study demonstrates that incorporating anthropometric variations in tibial and femoral segment lengths significantly influences the cortical strains in lower extremities in far-side impacts. A strong positive linear relationship was observed, with longer tibiae associated with higher strain levels in the cortical bone of the lower extremities, underscoring the importance of including anthropometric diversity in injury biomechanics research. However, the injury risk prediction remained unaffected – proximal tibia fractures were predicted with nearly 100% risk in all iterations, highlighting the robustness of the VIVA+ 50F in capturing lower extremity injury risk. Variations in tibial length were associated with changes in both the point and trajectory of impact, which in turn affected the local loading conditions and cortical bone strain. While shorter tibial lengths increased the likelihood of isolated rib fractures, the relationship between tibial length and the risk of multiple rib fractures is not linear and may be affected by other biomechanical or anthropometric factors.

Using real-world accidents to validate HBMs poses challenges, since detailed anthropometries such as tibial length remain usually unknown. The current study shows that an iteration in between anthropometric meaningful variations should be performed to study the robustness of the results.

Since lower extremity lengths differ in the current HBMs, differences in overall occupant kinematics and lower extremity strains are to be expected, emphasising the need for harmonisation or testing across a holistic sample of different anthropometries, or even better, varying the lengths within the virtual testing load cases.

VI. ACKNOWLEDGEMENTS

The authors would like to acknowledge the use of high performance computing resources provided by the IT Services (ZID) of Graz University of Technology.

VII. REFERENCES

[1] Euro NCAP. “Euro NCAP 2030 Roadmap: A Vision for Safer Mobility”, https://cdn.euroncap.com/media/74468/euro-ncap-roadmap-vision-2030.pdf. [cited 2025-03-22]

[2] Boström, O., Gabler, H.C., Digges, K., Fildes, B., Sunnevang, C. (2008) Injury Reduction Opportunities of Far Side Impact Countermeasures. *Proceedings of the 52nd Annual Scientific Conference of the Association for the Advancement of Automotive Medicine*, 2008, Toronto, Canada.

[3] Pattimore, D., Ward, E., Thomas, P., Bradford, M. (1991) The Nature and Cause of Lower Limb Injuries in Car Crashes. SAE Transactions. SAE Transactions, **100**: pp.1947–1958.

[4] Banglmaier, R., Rouhana, S., Beillas, P., Yang, K. (2003) Lower Extremity Injuries in Lateral Impact: A Retrospective Study. *Proceedings of the 47th Annual Meeting, Association for the Advancement of Automotive Medicine,* 2003, Lisbon, Portugal.

[5] Klug, C., Rudd, R., et al. (2022) Priorities in Far-side Protection - What can we learn from field data for the development of virtual testing protocols?. *Proceedings of the IRCOBI Conference*, 2022, Porto, Portugal.

[6] Pipkorn, B., Larsson, K., et al. (2018) Occupant Protection in Far-Side Impacts*. Proceedings of the IRCOBI Conference*, 2018, Athens, Greece.

[7] Perez-Rapela, D., Markusic, C., et al. (2018) Comparison of WorldSID to PMHS kinematics in far-side impact. *Proceedings of the IRCOBI Conference*, 2018, Athens, Greece.

[8] Perez-Rapela, D., Donlon, J.P. et al. (2021) Occupant Restraint in Far-Side Impacts: Cadaveric and WorldSID Responses to a Far-Side Airbag. Annals of Biomedical Engineering, **49**: pp.802–811.

[9] Pintar, F. A., Yoganandan, N., et al. (2007) Comparison of PMHS, WorldSID, and THOR-NT responses in simulated far side impact. Stapp Car Crash Journal, **51**: pp.313–360.

[10] Euro NCAP. “Far-Side Impact”, https://www.euroncap.com/en/car-safety/the-ratings-explained/adult-occupant-protection/lateral-impact/far-side-impact. [cited 2025-02-25]

[11] Perez-Rapela, D., Markusic, C., Whitcomb, B., Pipkorn, B., Forman, J., Crandall, J. (2019) Comparison of the simplified GHBMC to PMHS kinematics in far-side impact. *Proceedings of the IRCOBI Conference,* 2019, Florence, Italy.

[12] Bahouth, G.T., Murakhovskiy, D., Digges, K.H., Rist, H., Wiik, R. (2015) Opportunities for reducing far-side casualties. *Proceedings of the 24th International Technical Conference on the Enhanced Safety of Vehicles*, 2015, Gothenburg, Sweden.

[13] Brumbelow, M.L., Mueller, B.C., Arbelaez, R.A. (2015) Occurrence of serious injury in real-world side impacts of vehicles with good side-impact protection ratings*.* Traffic Injury Prevention, **16**(1): pp.125–132.

[14] Pipkorn, B., Östh, J., et al. (2021) Validation of the SAFER Human Body Model Kinematics in Far-Side Impacts*. Proceedings of the IRCOBI Conference*, 2021, Lisbon, Portugal.

[15] John, J., Klug, C., Kranjec, M., Svenning, E., Iraeus, J. (2022) Hello, world! VIVA+: A human body model lineup to evaluate sex-differences in crash protection. Frontiers in bioengineering and biotechnology, **10***:* p.918904.

[16] Arun, M. W., Umale, S., Humm, J. R., Yoganandan, N., Hadagali, P., Pintar, F. A. (2016) Evaluation of kinematics and injuries to restrained occupants in far-side crashes using full-scale vehicle and human body models. Traffic Injury Prevention*,* **17**(1): pp.116–123.

[17] Parham, J.L., Paquette, S.P. (2017) Natick Soldier Research, Development and Engineering Center, *2012 US Army Anthropometric Working Databases (ANSUR II)*, Natick, MA, USA.

[18] Fildes, B.N., Sparke, L.J., Boström, O., Pintar, F., Yoganandan, N., Morris, A.P. (2002) Suitability of Current Side Impact Test Dummies in Far-Side Impacts. *Proceedings of the IRCOBI Conference*, 2002, Munich, Germany.

[19] Bruna-Rosso, C., Wei, W., Bourdet, N., Serre, T., Arnoux, P.-J. (2025) From crash data to a "virtual injury assessment". International Journal of Crashworthiness: pp.1–8.

[20] Steffan, H., Moser, A., Ambros, J. (2004) PC-Crash – A Simulation Program for Vehicle Accidents. *Proceedings of the IRCOBI Conference*, 2004, Graz, Austria.

[21] Fichera, C., Flannagan, C., John, J. (2024) Quantifying Sex-Differences in Anthropometry: A Bayesian Approach. *Proceedings of the IRCOBI Conference*, 2024, Stockholm, Schweden.

[22] Iraeus, J., Lindquist, M**.** (2016) Development and validation of a generic finite element vehicle buck model for the analysis of driver rib fractures in real-life nearside impacts. Accident Analysis & Prevention, **86**: pp.125–134.

[23] Euro NCAP. (2022) "Far Side Test and Assessment Protocol Version 2.3". [cited 2023-01-15]

[24] Fitterer, S., Ressi, F., Steffan, H., and Klug, C. (2023) Simulation study of a real-world far-side crash. *Proceedings of the IRCOBI Conference*, 2023, Cambridge, UK.

[25] International Organization for Standardization (ISO). "ISO/TS 18571:2024 – Road vehicles – Objective rating metric for non-ambiguous signals", https://www.iso.org/standard/85791.html. [cited 2025-22-03]

[26] Hotzman, J., Gordon, C.C., et al. (2011) U.S. Army Army Natick Soldier Research, Development and Engineering Center, *Measurer's Handbook: US Army and Marine Corps Anthropometric Surveys*, 2010-2011, Natick, MA, USA.

[27] Gordon, C.C, Churchill, T., et al. (2014) U.S. Army Army Natick Soldier Research, Development and Engineering Center, *2012 Anthropometric Survey of U.S. Army Personnel (ANSUR II): Methods and Summary Statistics*, Natick, MA, USA.

[28] Tezzele, M., Demo, N., Mola, A., Rozza, G. (2021) PyGeM: Python Geometrical Morphing. Software Impacts, **7:** p.100047.

[29] Burstein, A.H., Reilly, D.T., Martens, M. (1976) Aging of Bone Tissue: Mechanical Properties. The Journal of Bone and Joint Surgery, **58**(1): pp.82–86.

[30] Ding, M. (2000) Age variations in the properties of human tibial trabecular bone and cartilage. Acta Orthopaedica, **71**(292): pp.i-45.

[31] Erlinger, N., Iraeus, J., John, J., Klug, C. "Human Body Models for lower extremity fracture prediction in car to pedestrian crashes representing the average female and male", https://openvt.eu/fem/viva/vivaplus-validation/-/blob/0beff09d5a232b935949db8fa699a0c5f52698d8/catalog/Harden-2021-Tibia-shaft/Harden-2021.ipynb. [cited 2025-03-25]

[32] Larsson, K.J., Blennow, A., Iraeus, J., Pipkorn, B., Lübbe, N. (2021) Rib Cortical Bone Fracture Risk as a Function of Age and Rib Strain: Updated Injury Prediction Using Finite Element Human Body Models. Frontiers in Bioengineering and Biotechnology, **9**: p.677768.

[33] Harden, A.L., Kang, Y.S., et al. (2021) Preliminary sex-specific relationships between peak force and cortical bone morphometrics in human tibiae subjected to lateral loading. *Proceedings of the IRCOBI Conference*, 2021, online.

[34] Schubert, A., Erlinger, N., Leo, C., Iraeus, J., John, J., Klug, C. (2021) Development of a 50th Percentile Female Femur Model. *Proceedings of the IRCOBI Conference*, 2021, online.

VIII. APPENDIX

A) Material Validation with ISO 18571 Rating

TABLE A-I
SLIDING SCALE OF THE OVERALL ISO RATING

Rank, *r*	Grade	Rating, *R*	Description
1	Excellent	R > 0,94	Almost perfect characteristics of the reference signal is captured
2	Good	0,80 < R ≤ 0,94	Reasonably good characteristics of the reference signal is captured, but there are noticeable differences between both signals
3	Fair	0,58 < R ≤ 0,80	Basic characteristics of the reference signal is captured but there are significant differences between the two signals
4	Poor	R ≤ 0,58	Almost no correlation between the two signals

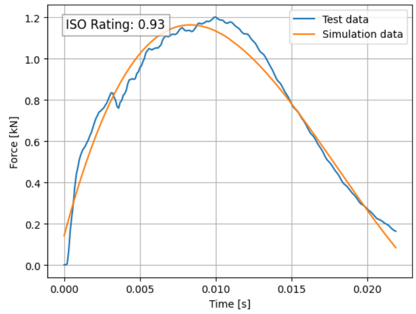

Fig. A-1 Test data vs. Simulation data for MP1.

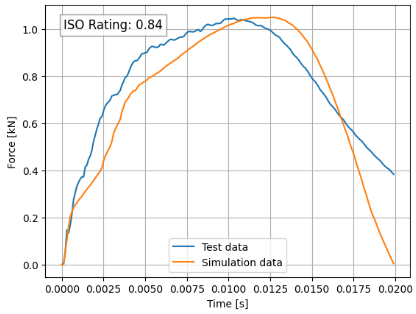

Fig. A-2. Test data vs. Simulation data for MP2.

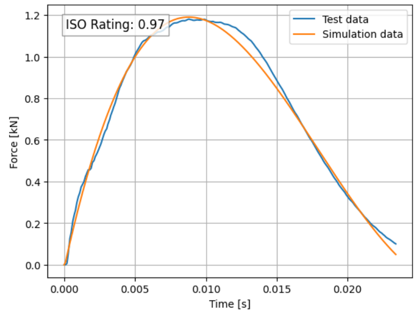

Fig. A-3. Test data vs. Simulation data for MP3.

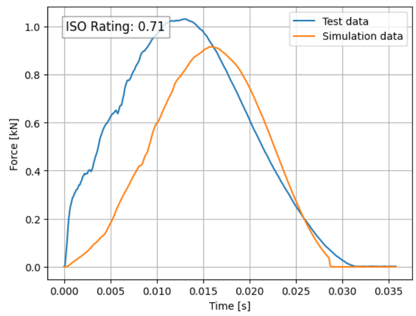

Fig. A-4. Test data vs. Simulation data for MP4.

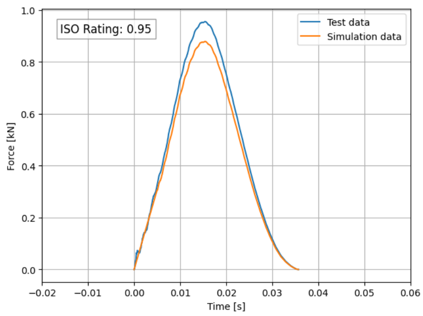

Fig. A-5. Test data vs. Simulation data for MP5.

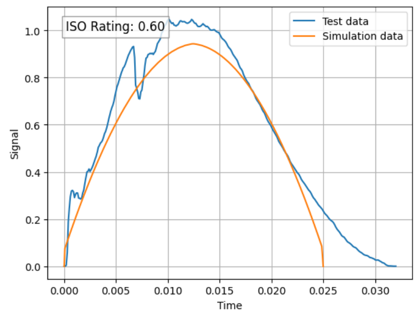

Fig. A-6. Test data vs. Simulation data for MP6.

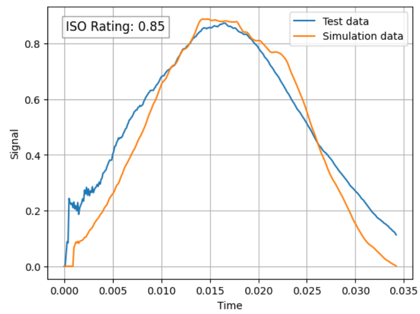

Fig. A-7. Test data vs. Simulation data for MP7.

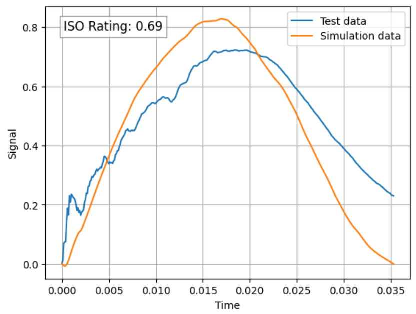

Fig. A-8. Test data vs. Simulation data for MP8.

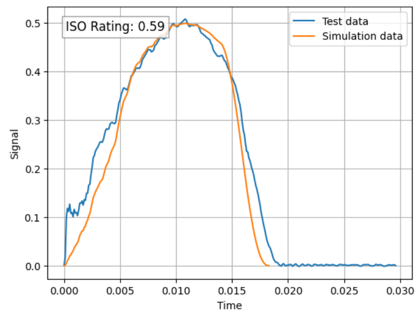

Fig. A-9. Test data vs. Simulation data for MP9.

B) Bayesian Linear Regression Model – Results

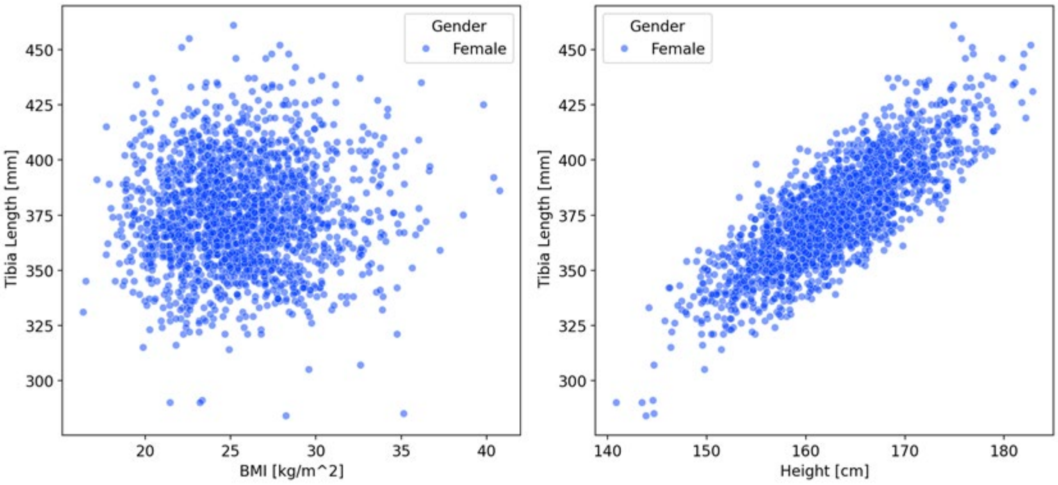

Fig. B-1. Calculated tibial lengths from the ANSUR female dataset in relation to BMI and height.

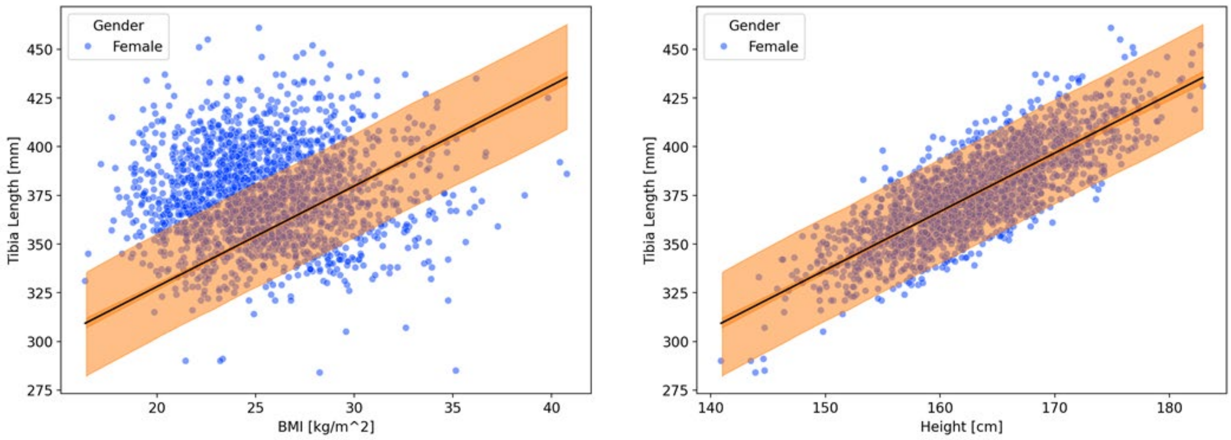

Fig. B-2. Visualisation of the Bayesian linear regression results for tibial length as a function of BMI and height, incorporating observed data, posterior predictions, and uncertainty intervals.

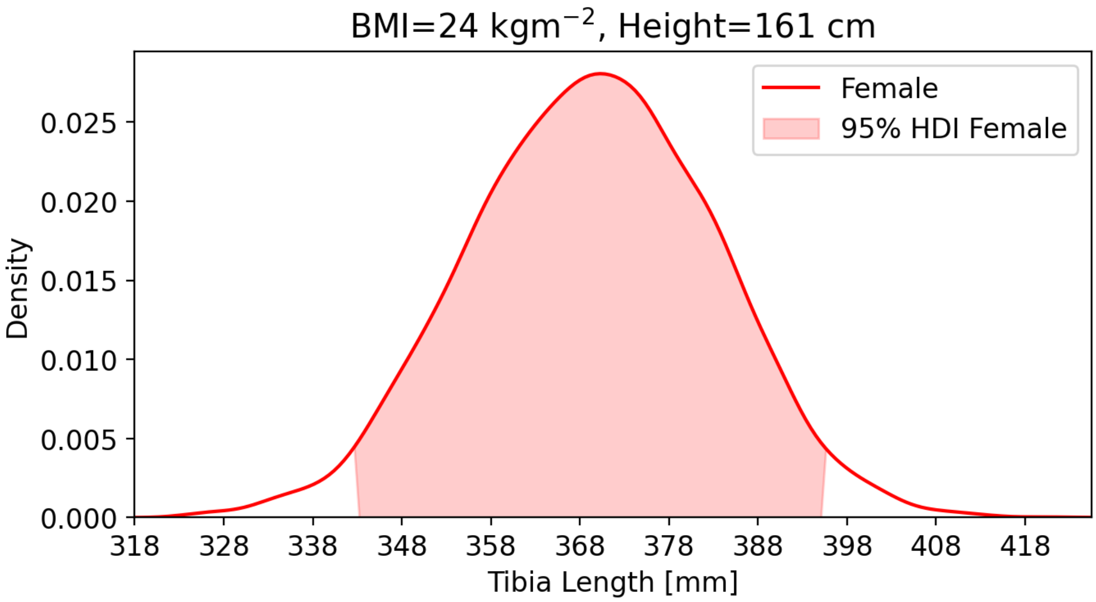

Fig. B-3. Estimated range of tibial lengths in 95% high density interval (HDI) based on Bayesian linear regression results (95% HDI: 342.66 - 395.18 mm).

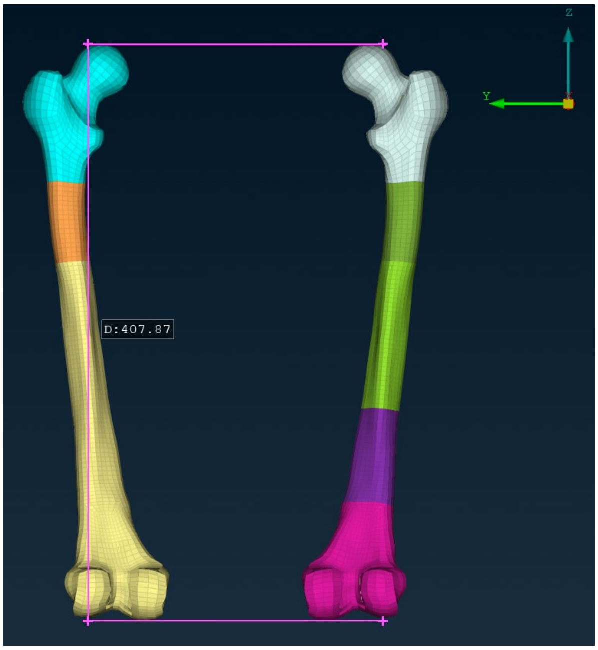

Fig. B-4. Measured femoral length of VIVA+ 50F (407.87mm).

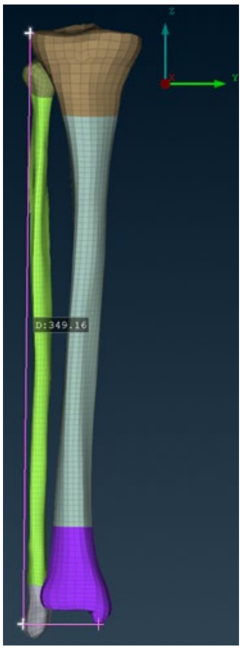

Fig. B-5. Measured tibial length of VIVA+ 50F (349.16mm).

TABLE B-I
ESTIMATED TIBIAL AND FEMORAL LENGTHS BASED ON BAYESIAN LINEAR REGRESSION MODEL

	Tibial Length Variation (mm)	VIVA+50F Total Leg Length (757.03mm) → Total Leg Length - Tibial Length	Resulting Femoral Length (mm)
95% HDI Tibial Length Range: 342.66 - 395.18mm	*342.66*	757.03-342.66	414.37
	347.91	757.03-347.91	409.12
	349.16	757.03-349.16	407.87
	353.16	757.03-353.16	403.87
	358.41	757.03-358.41	398.62
	363.66	757.03-363.66	393.37
	368.91	757.03-368.91	388.12
	374.16	757.03-374.16	382.87
	384.66	757.03-384.66	372.32
	395.16	757.03-395.16	361.87

C) Maximum Principal Strains of right Tibia

TABLE C-I
MEASURED TIBIAL CORTICAL STRAINS (MPS)

Tibial Length [mm]	Resulting Femoral Length [mm]	Measured Strain Value [-]
342.66	414.37	0.063654542
347.91	409.12	0.059431737
349.16	407.87	0.059295069
353.16	403.87	0.060409419
358.41	398.62	0.061185024
363.66	393.37	0.058856495
368.91	388.12	0.056803855
374.16	382.87	0.059430899

D) *Tibia Kinematics*

TABLE D-I

CONTACT KINEMATICS OF PROXIMAL LATERAL TIBIA WITH INSTRUMENT PANEL

Tibial Length [mm]	Initial Contact Time [ms]	Contact Duration [ms]	Max Y-Force [kN]
342.66	47.99	95.99	5.7625
347.91	47.99	96.02	6.2233
349.16	47.99	97.00	6.2164
353.16	47.99	97.99	6.4258
358.41	46.99	99.99	6.5917
363.66	46.99	98.99	6.6202
368.91	46.99	98.99	7.1641
374.16	46.99	99.99	7.4463

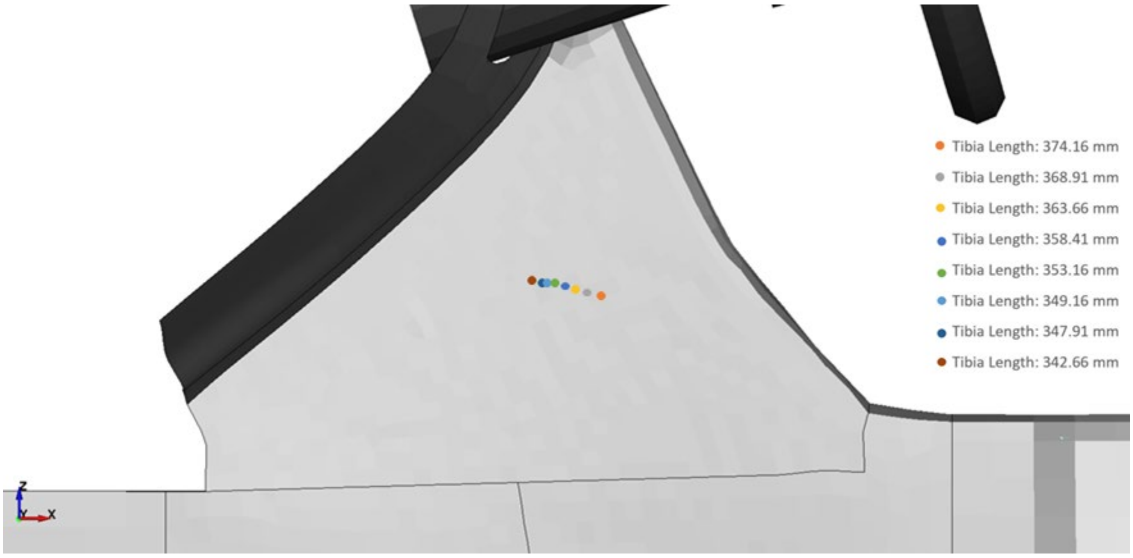

Fig. D-1. Contact points of right lateral tibial condyles at initial contact with instrument panel.

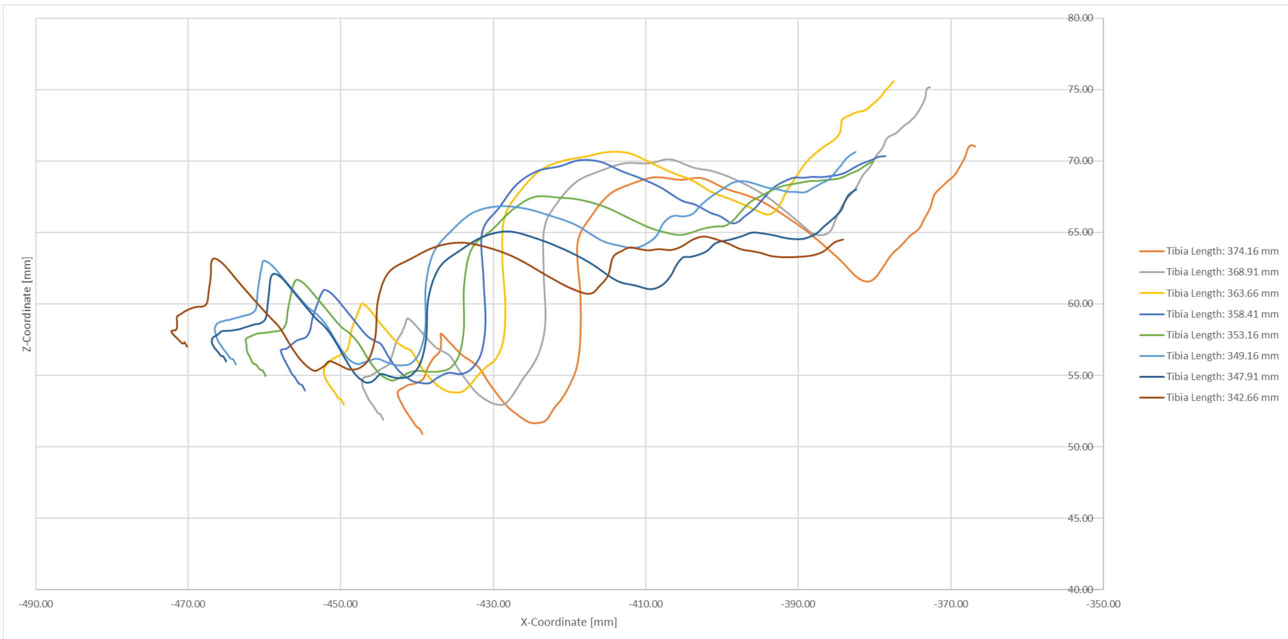

Fig. D-2. XZ-Trajectories of right lateral tibial condyles during contact with instrument panel.

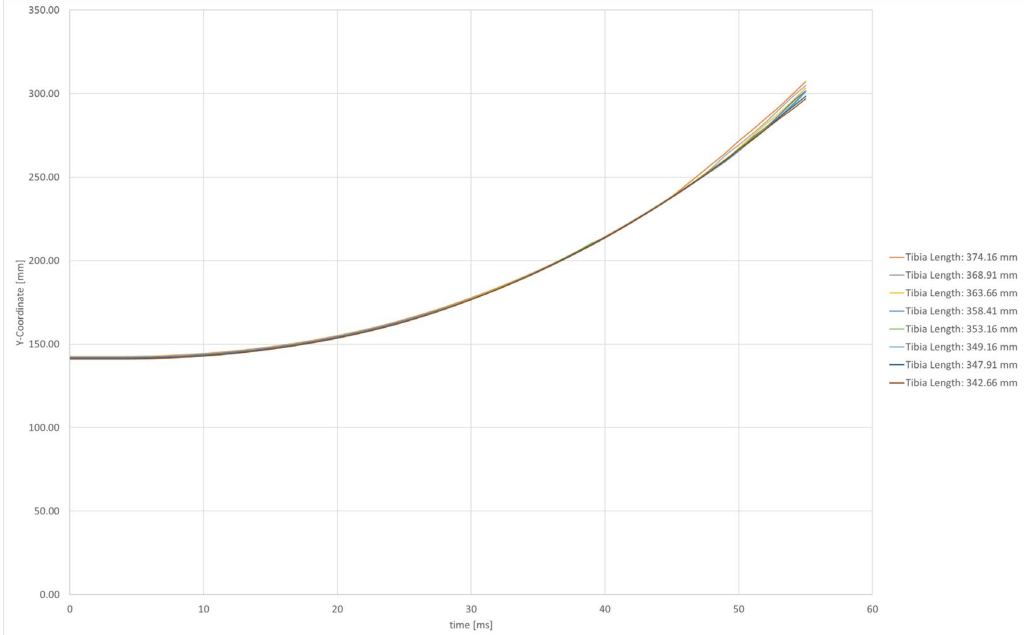

Fig. D-3. YZ-Trajectories of right lateral tibial condyles during contact with instrument panel.

E) Fracture Risk Tibia and Femur

The injury risk curve for fracture of the VIVA+ model's tibia shaft was created by [32] using test data by [33]. The methodology was based on the approach used for the femur risk curve developed by [34]. A corresponding manuscript is currently in preparation for release. A Jupyter notebook with all calculations and injury risk curves is available at OpenVT (https://openvt.eu/fem/viva/vivaplus-validation/-/blob/main/catalog/Harden-2021-Tibia-shaft/Harden-2021.ipynb).

Currently, no specific Injury Risk Curve (IRC) for tibial head fracture for the VIVA+ models is available. While not ideal, the decision was made to use the fracture risk curve for the tibia shaft in the absence of an alternative, emphasising the need for dedicated injury risk curves tailored to relevant bone regions. All fracture risk values for tibia and femur are summarised in tables E-I and E-II.

TABLE E-I
FRACTURE RISK OF RIGHT TIBIA

Tibial Length [mm]	Tibia 99th PS Fracture Risk [%]	Tibia MPS Fracture Risk [%]
342.66	99.99	99.99
347.91	99.99	99.99
349.16	99.99	99.99
353.16	99.99	99.99
358.41	99.99	99.99
363.66	99.99	99.99
368.91	99.99	99.99
374.16	99.99	99.99

TABLE E-II
FRACTURE RISK OF RIGHT FEMUR

Tibial Length [mm]	Femur 99th PS Fracture Risk [%]	Femur MPS Fracture Risk [%]
342.66	76.17	74.33
347.91	76.95	74.19
349.16	76.33	73.06
353.16	77.63	75.77
358.41	79.50	78.81
363.66	79.31	77.88
368.91	79.30	77.66
374.16	79.23	77.80